Bulletin of the Seismological Society of America, Vol. 106, No. 5, pp. –, October 2016, doi: 10.1785/0120160045

Ⓔ

Moment Magnitudes of Local/Regional Events from 1D Coda Calibrations in the Broader Middle East Region

by Rengin Gök, Ayoub Kaviani, Eric M. Matzel, Michael E. Pasyanos, Kevin Mayeda, Gurban Yetirmishli, Issa El-Hussain, Abdullah Al-Amri, Farah Al-Jeri, Tea Godoladze, Dogan Kalafat, Eric A. Sandvol, and William R. Walter

Abstract Reliable moment magnitude estimates for seismic events in the Middle East region can be difficult to obtain due to the uneven distribution of stations, the complex tectonic structure, and regions of high attenuation. In this study, we take advantage of the many new broadband seismic stations that have become available through improved national networks and numerous temporary deployments. We make coda envelope-amplitude measurements for 2247 events recorded by 68 stations over 13 narrow frequency bands ranging between 0.03 and 8 Hz. The absolute scaling of these spectra was calculated based on independent waveform modeling solutions of the moment magnitudes for a subset of these events to avoid circularity. Using our 1D path calibrations, we determined coda-based magnitudes for a majority of the events. We obtain fairly good agreement with waveform-modeled seismic moments for the larger events ($M_w > 4.5$) at low frequencies (< 0.7 Hz). As expected, the coda-derived source spectra become increasingly scattered at higher frequencies (> 0.7 Hz) because of unaccounted 2D path effects, as well as mixing of both *Sn* coda and *Lg* coda, which have different attenuation behavior. This scatter leads to increased variance in the magnitudes estimated for smaller events in which low-frequency amplitudes are below the noise levels and the higher frequencies are the only signals available. We quantify the expected variance in coda envelope amplitudes as a function of frequency using interstation scatter as our metric. The net results of this study provide thousands of new 1D coda magnitude estimates for events in the broad region, as well as the necessary initial starting model for use in a new related 2D coda study (Pasyanos *et al.*, 2016).

Online Material: Table of site terms and moment magnitudes.

Introduction

Moment magnitude estimation for seismic events in tectonically diverse regions is very challenging due to the effects of strong structural variations that are not necessarily well-modeled with a simple 1D velocity and attenuation structure. In this study, we utilize national network data to enable better estimates of seismic source parameters in the broader Middle East region. For sparse local and regional seismic networks, a stable moment magnitude is quite important for establishing accurate seismicity catalogs and assessing seismic-hazard potential. Accurate magnitude and source parameters are also critical for construction and formation of regional attenuation parameters. Unlike other types of magnitudes such as M_L, m_b, and M_s that often have biases due to regional propagation differences, the empirical coda envelope approach (Mayeda and Walter, 1996; Mayeda *et al.*, 2003) can provide stable absolute source spectra that are corrected for *S*-to-coda transfer function, scattering, anelastic attenuation, and site effects. In previous studies, we found that the coda envelope-amplitude measurements were not very sensitive to 3D path heterogeneity (at lower frequencies) and source radiation pattern, provided that ample duration was available for the amplitude measurements (e.g., Mayeda and Malagnini, 2010). Because of the scattering nature of the coda, amplitudes derived from the envelopes average over the path and source variation. The resultant source spectra were used to calculate stable moment estimates (and hence M_w) and were later compared with traditional magnitudes (M_L, m_b, and M_s), as well as radiated seismic energy. In this study, we use the 1D coda-derived spectra that are dominated by scattered surface waves at longer periods and scattered *Sn* and/or *Lg* waves at regional distances, as

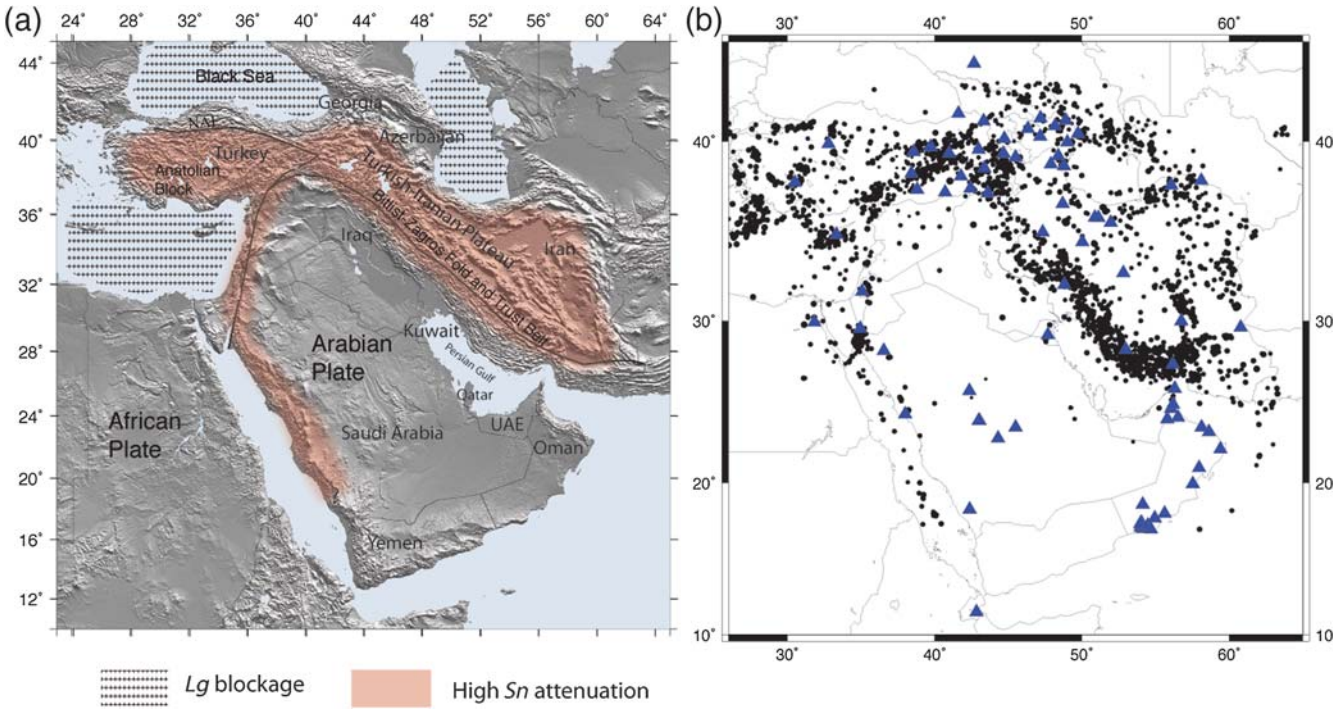

Figure 1. (a) Tectonic setting and *Lg*, *Sn* propagation in the region (NAF, North Anatolian fault zone). The thick gray line is the plate boundary. (b) Events (solid circles) and stations (blue triangles) that were used in this study. Ⓔ Magnitudes will be available in the electronic supplement to this article.

well as scattered direct *S* waves at local distances. Our goal is to provide a large set of calibrated quality-assessed moment magnitudes of nearly 2247 small-to-large size earthquakes that span $3.5 < M_w < 7.0$.

Although the coda envelopes are robust over a large frequency range, at higher frequencies (> 0.7 Hz) the regional *S*-wave characteristics influence the coda envelope calibrations. The *Sn* phase is a high-frequency guided seismic wave that travels in the lithospheric mantle with a typical frequency of 1–4 Hz or more. The typical velocity for *Sn* is around 4.5 km/s in stable continental and oceanic lithosphere. *Lg* is shown to be sensitive to lateral changes in the crust and travels with a velocity between 3.2 and 3.7 km/s. These variations affect the 1D coda start time calibrations, which we clearly demonstrate in the Method section.

The *Lg* coda typically constitutes the most prominent phase observed on regional-distance seismograms recorded from crustal events traveling over continental paths. The *Lg* coda is widely used for local and regional attenuation studies for stable *Q* estimates (Aki and Chouet, 1975; Cong and Mitchell, 1998). In active tectonic regions, direct *Lg* waves are highly attenuated. Molnar and Oliver (1969), followed by Kadinsky-Cade *et al.* (1981), observed very weak *Sn* propagation in the Iranian–Turkish plateau. The same study demonstrates that *Lg* is also absent or weak on the seismograms with paths crossing the plateau and across the south Caspian Sea. Later studies by Mitchell *et al.* (1997), Rodgers *et al.* (1997), and Cong and Mitchell (1998) confirmed the same results (Fig. 1a). The more detailed studies by Sandvol *et al.* (2001), Gök *et al.* (2003), and Al-Damegh *et al.* (2004) indicate *Lg* blockage across the Bitlis suture and the Zagros fold-and-thrust belt and weak *Lg* and *Sn* propagation in most of the Iranian–Turkish plateau (Baumgardt, 2001; Fig. 1). Kaviani *et al.* (2015) present detailed crustal attenuation and velocity models for the northern Middle East using *Lg* waves recorded by a very dense network. The tomographic models presented by Kaviani *et al.* (2015) show lower values of *Lg* Q_0 over the Turkish–Anatolian plateau (< 150) than those observed over the Iranian plateau (150–400).

Direct wave amplitude measurements are affected by source radiation pattern, directivity, and heterogeneities along the path, which causes large amplitude variability (e.g., Favreau and Archuleta, 2003). Previous studies have compared direct waves with coda waves (e.g., Mayeda, 1993; Mayeda and Walter, 1996; Mayeda *et al.*, 2003; Eken *et al.*, 2004; Malagnini *et al.*, 2004), and all have found that amplitude measurements of direct waves are 3–5 times more variable than coda amplitudes. We demonstrate in this study that 1D coda-derived magnitudes provide great stability, due to their averaging nature at frequencies of 0.7 Hz and lower, and thus are applicable for events $M_w \geq \sim 4.0$ for this region. However, for smaller events, best observed above 0.7 Hz, it is clear that 2D path effects become significant, and a simple 1D path correction results in a more uncertain magnitude estimate. This study will provide an initial 1D starting model for a future 2D coda amplitude tomography that we believe will allow for more stable moment magnitudes down to M_w 3.0 or lower. With increased understanding of the frequency-specific

variability in 1D corrected coda amplitudes and its impact on the uncertainty in the magnitude estimates, we will be able to provide recommendations for national networks with magnitude reporting requirements. Using these recommendations, national networks will be able to use this powerful and easy-to-implement methodology at uncertainty levels that are better than other traditional magnitudes. We also provide a relationship between M_w and traditional magnitudes (M_L, m_b, and M_s) to be used for the completeness and harmonization part of the probabilistic seismic-hazard assessment (PSHA).

Data

We analyzed waveforms from 68 seismic stations consisting of permanent and temporary stations in the region (Fig. 1b). All stations were three-component broadband from national networks or open data sources (wherever available). Station selection criteria were also based on geographical distribution and homogeneity. Because coda waves provide an averaging effect along the path, many studies showed that even single-station moment magnitudes are very close to the network average of direct waves (e.g., Mayeda *et al.*, 2003). We obtained a large number of crustal (depth < 33 km) events out to a distance of ~14°, where most of the seismic activity is associated with major plate boundaries or the Turkish and Iranian plateaus (e.g., Bitlis–Zagros fold-and-thrust belt, Red Sea, Makran). We used the preferred origin information for each event from our database, which is composed of locations from International Seismic Centre (ISC), National Earthquake Information Center (NEIC), and other regional bulletin providers. In the Arabian Peninsula, the numbers of events are limited compared with the Turkish and Iranian plateaus. The use of data from so many institutions in the broader Middle East region, including data from Incorporated Research Institutions for Seismology-Program for the Array Seismic Studies of the Continental Lithosphere (IRIS-PASSCAL) deployments, International Institute of Earthquake Engineering and Seismology (IIEES), Republic Seismic Survey Center of Azerbaijan (RCSS), Earthquake Monitoring Center (EMC) of Sultan Qaboos University, King Abdullah City of Science and Technology (KACST), Kandilli Observatory and Earthquake Research Institute (KOERI), Kuwait Institute of Scientific Research (KISR), and Saudi Geological Survey (SGS), provided the most complete coverage for any magnitude study that we are aware of in this region.

Method

Instrument-corrected regional broadband velocity seismograms were used in the coda calibration following the method outlined by Mayeda *et al.* (2003). The result is coda-derived moment-rate spectra that are tied to independent waveform-modeled moments. The coda technique described here has been widely used for regional calibrations, sometimes with very few stations. Years of accumulated data from different networks have allowed us to expand the coda envelope database. It should be noted here that coda calibrations can be calculated using various advanced techniques. However, we are using the simple description of the coda start and decay parameters to be able to make use of a wide variety of networks ranging from very sparse ones to those with a large number of stations. The following outlines the calibration method, and more in-depth information can be found in Mayeda *et al.* (2003).

The coda envelope $A_c(f,t,r)$ is defined as

$$A_c(f,t,r) = W_0(f) \times S(f) \times T(f) \times P(r,f) \times H\left(t - \frac{r}{v(f,r)}\right) \times \left(t - \frac{r}{v(f,r)}\right)^{-\gamma(f,r)} \exp\left[b(f,r) \times \left(t - \frac{r}{v(f,r)}\right)\right], \quad (1)$$

in which f is the center frequency, r is the epicentral distance in kilometers, t is the time in seconds from the origin time, v is the peak velocity (in km/s), W_0 represents the S-wave source, T represents the S-to-coda transfer function, S is the site effect, P includes the effects of geometrical spreading and attenuation, H is the Heaviside step function, and $\gamma(r)$ and $b(r)$ are the distance-dependent coda shape factors that control the coda envelope shape. By ignoring the source, path, site, and transfer function effects, the equation becomes

$$\log_{10}\left[A_c(f,t,r) \times \left(t - \frac{r}{v(f,r)}\right)^{\gamma(f,r)}\right] = \log_{10}\left[H\left(t - \frac{r}{v(f,r)}\right)\right] + b(f,r) \times \left(t - \frac{r}{v(f,r)}\right) \times \log_{10}(e). \quad (2)$$

We start by forming 13 narrowband envelopes (ranging from 0.03 to 8 Hz) of instrument-corrected horizontal components (north–south and east–west) at epicentral distances ranging between 1° and 14°. Envelopes generated via Hilbert transform technique were smoothed at a varying number of samples (higher smoothness factor $h = 10$ at low frequencies gradually decreasing down to $h = 2$ for the highest frequency band). We then measure the maximum peak velocity within the group velocity window of 4.7–2.3 km/s for $\Delta > 300$ km and 3.9–1.9 km/s for $\Delta \leq 300$ km epicentral distance. The selection of the peak time of the direct phase is measured automatically by selecting the largest envelope amplitude at a signal-to-noise ratio (SNR) ≥ 1.2 (Fig. 2). The noise window is selected 5 s prior to the P arrival time. There are some false detections seen at unrealistic group velocities, because the low SNR allows spurious data points. Some of the peak velocity values are also the result of *Sn*-to-*Lg* conversions (4.0–4.3 km/s) at boundaries between oceanic and continental crust in the Mediterranean Sea, Black Sea, and Caspian Sea. After measuring all of the peak amplitude arrivals, we obtained the envelope peak velocity function that is represented with a simple hyperbola. This function will be part of

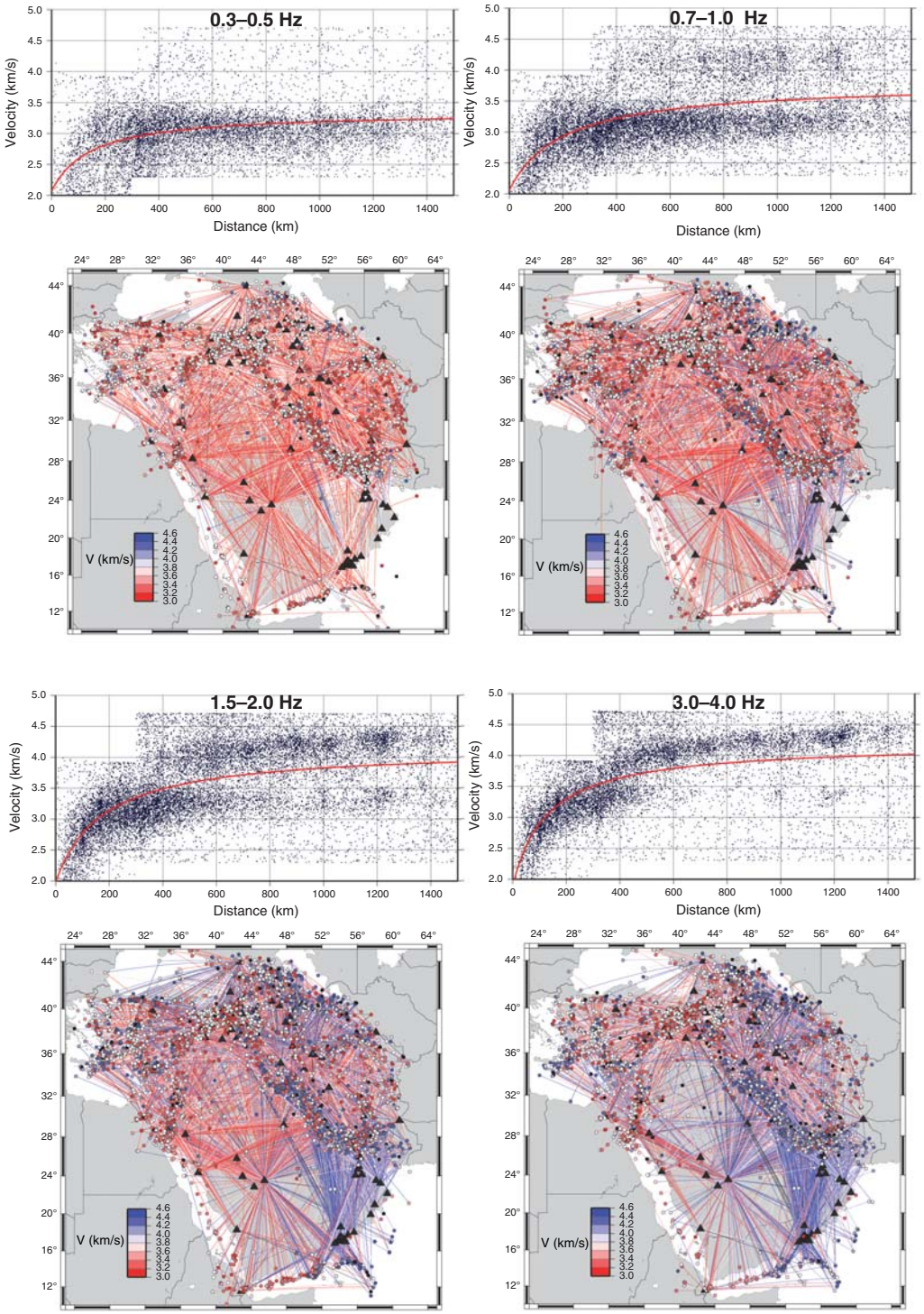

Figure 2. Automatically picked coda envelope peak velocities at selected frequency bands. Earthquakes are plotted as circles and color-coded for their velocities. The red hyperbola represents the best fit to the peak velocity distribution at the specific frequency band.

coda calibration and will also be used in future measurements in the region (red hyperbola in Fig. 2). The function is represented with

$$v(f, r) = v_0(f) - \frac{v_1(f)}{v_{2(f)} + r}, \qquad (3)$$

in which r is the epicentral distance and v_0, v_1, and v_2 are constants. In Figure 2, four different frequency-band peak velocities are shown. As the frequency gets higher, the scattering of the shape parameter increases. At 0.3–0.5 Hz, it is dominated by short-period surface waves (Rayleigh or Love) with an average velocity of around 3.0 km/s. At 0.7–1.0 Hz and

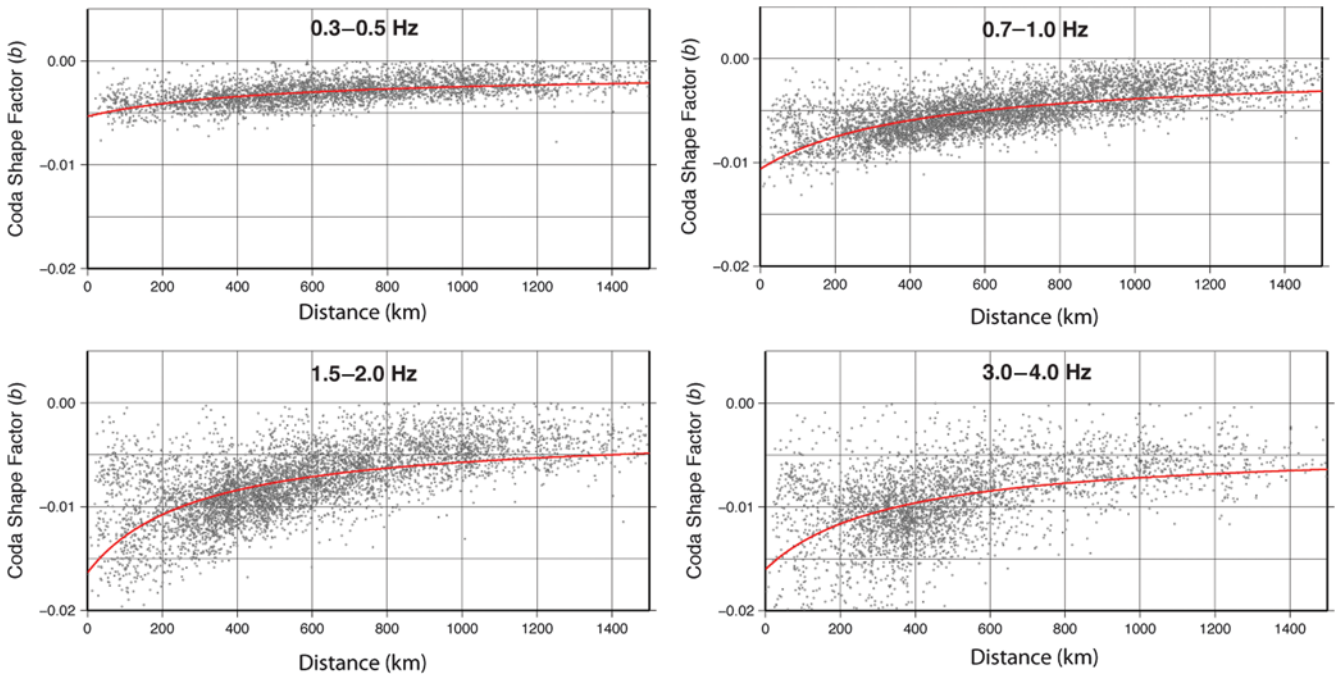

Figure 3. Coda shape function (parameter *b*, equation 4) at selected frequencies. The red hyperbola represents the best fit to the coda shape parameters at the specific frequency band. Note the increased variability at higher frequencies.

1.5–2.0 Hz, the predominant phase can be either *Sn* or *Lg*, as clearly indicated with a larger number of points accumulated around 4.5 and 3.7 km/s. At 3.0–4.0 Hz, the peak value is mostly dominated by *Sn* (4.5 km/s). *Sn* is observed with larger amplitude at high frequencies, and the *Lg* amplitude is eliminated at higher frequencies. Coda envelope window lengths were determined by manual inspection of the time window of the envelope. All envelopes were carefully inspected in order to avoid the effects of any aftershocks. The expectation of minimum and maximum window length was adopted from previous studies (Mayeda and Walter, 1996; Yoo *et al.* 2011) and slightly modified for the region. The window lengths change as a function of frequency and depend on the attenuation structure in the region. If the selected coda window length is too short, then there is a bias of estimating the coda amplitude in the very early part of coda due to low SNR. Coda windows tend to last very long for very large events ($M_w > 7.0$). We eliminate those cases by limiting the maximum window length criteria.

The shapes of the coda envelopes are represented by the following functional forms:

$$b(f,r) = b_0(f) - \frac{b_1(f)}{b_2(f) + r} \tag{4}$$

and

$$\gamma(f,r) = \gamma_0(f) - \frac{\gamma_1(f)}{\gamma_2(f) + r}, \tag{5}$$

which have been empirically demonstrated to provide a reasonable fit of the envelopes as a function of increasing distance. Figure 3 shows the *b*-value and the estimated hyperbola (equation 4) at four different frequencies. The coda shape parameter does not seem to vary much at local to near-regional distances (< 200 km) below 0.5–0.7 Hz. However, as frequencies increase, the shape parameter seems to show increasing variation at local distances. The 3.0–4.0 Hz band seems to exhibit very large variation at larger epicentral distances. We have fewer shape measurements than the peak values, due to rejection for window lengths. Figure 4 shows these variations when compared with the synthetic envelopes.

Figure 4 shows the observed coda envelopes along with empirical synthetic envelopes. Coda amplitudes are measured by statistically shifting the synthetic envelopes that were created for a unit source. The envelope start and the shape functions were obtained from the hyperbolic functions (equations 4 and 5). In Figure 4a, thick gray and black synthetic envelopes were shifted to fit the amplitude level, and the coda measurements are made at 200 s for all frequencies (Scott Phillips, personal comm., 2016). The rationale for choosing this particular lapse time is to sample the same scattered ellipsoid at a particular time in the coda.

In Figure 4a, we show an event recorded at stations RAYN (Saudi Arabia) and ASAO (Iran) at 1.0–1.5 Hz frequency band. In Figure 4b, the synthetic envelopes at 825 km are shown for all frequencies. The shape functions and the start times are obtained from Table 1. Note in particular that station ASAO has a peak velocity associated with *Sn*, whereas station RAYN has an *Lg* associated velocity (Fig. 4a). Given this, it is all the more remarkable that the shapes are otherwise similar except for an offset of 0.3 log units. The site term for RAYN at 1.0–1.5 Hz is 19.388, whereas it is 20.029 for ASAO (see Ⓔ Table S1, available in the electronic

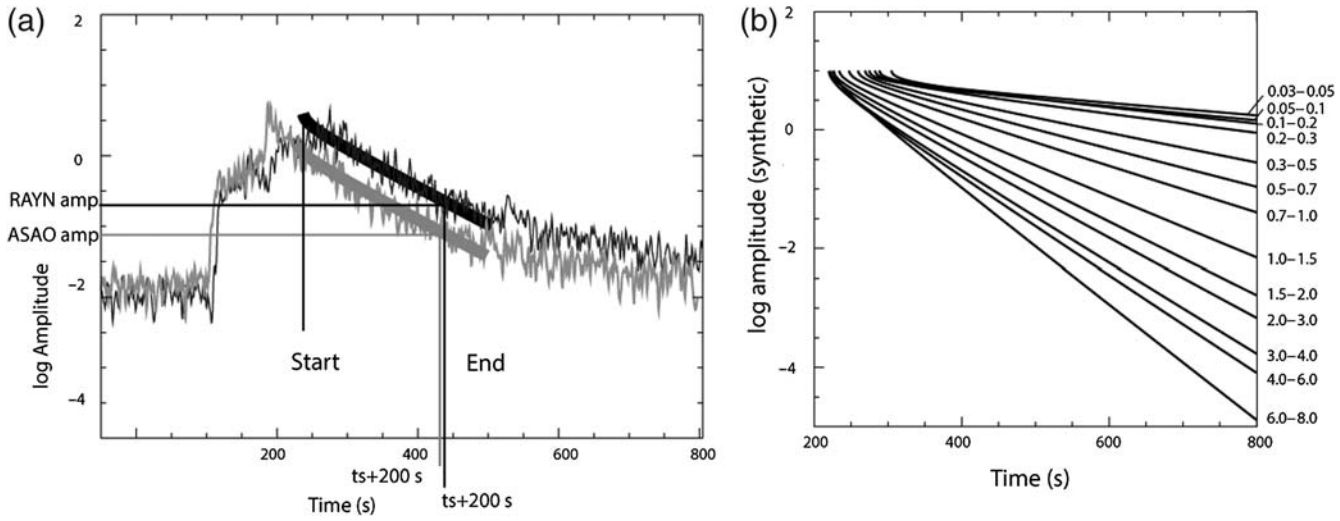

Figure 4. (a) An example of coda envelopes and synthetics (thick line) recorded at stations RAYN (black) and ASAO (gray) at 1.0–1.5 Hz frequency band (event from Fig. 9a, southern Zagros [SZ]). (b) Synthetic envelopes of all frequency bands at 825 km distance is shown for the same event (right).

supplement to this article). The difference of 0.641 in site terms accounts for much of this difference, with Q path variations accounting for the rest. The start time and the shape functions were obtained from Table 1. The 22 March 2005 event (M_w 4.21) envelopes for 1.0–1.5 Hz frequency band are shown for ASAO (gray) and RAYN (black) and the synthetics (thick black and gray lines).

After all of the amplitudes are collected from 68 stations at 13 frequency bands, we corrected for the path effect. It has generally been observed that attenuation of coda varies with frequency, tectonic region, and the lapse time interval used in the observations and tends to be lower in tectonically active regions and higher in inactive stable regions (Singh and Herrmann, 1983; Jin and Aki, 1988, 2005). We used the Extended Street and Herrmann (ESH) formulation, a modification of the Street *et al.* (1975) spreading function, in which both the geometrical spreading and the Q effect are corrected. ESH corrects for the geometrical spreading, and its results are more stable than those derived from using the Brune-like corrections at higher frequencies (Morasca *et al.*, 2008; Yoo *et al.*, 2011). Instead of one critical distance, they define a distance range in which the transition changes smoothly (Fig. 5):

$$f(r) = r^{-p_1} \quad r < X_1$$
$$f(r) = (X_1^{-p_1})(r/X_1)^{p_1+\Delta p(r)/2} \quad X_1 < r < X_2, \qquad (6)$$

in which

$$\Delta p(r) = \log(r/X_1)(p_2 - p_1)/\log(X_2/X_1)$$

$$f(r) = (X_1^{-p_1})(X_2/X_1)^{-(p_1+\Delta p(r)/2)}(r/X_2)^{-p_2} \qquad r > X_2,$$

in which

$$\Delta p(r) = (p_2 - p_1).$$

To minimize the interstation scatter between the stations, the inversion algorithm is applied using the following relations:

Table 1
Coda Calibration (1D) Parameters for Station UOSS

Frequency Band (Hz)	v_0	v_1	v_2	b_0	b_1	b_2	γ_0	γ_1	γ_2	p_1	p_2	x_c	x_t	Q	Site
0.03–0.05	3.10	12	201	−0.001	0.18	500	0.10	0	1	0.0000	1	1000	1.58	998711	21.98
0.05–0.1	2.95	14	201	−0.001	0.00	0	0.10	0	1	0.1320	1	829	1.33	996396	21.02
0.1–0.2	2.85	64	200	−0.001	0.52	500	0.10	−1	1	0.0639	1	496	2.88	263	20.42
0.2–0.3	3.25	250	201	−0.0005	1.56	499	0.10	0	1	0.2554	1	414	3.61	203	19.76
0.3–0.4	3.35	186	145	−0.001	2.14	500	0.10	0	1	0.6921	1	536	1.00	307	18.65
0.5–0.7	3.55	284	199	−0.0005	3.94	500	0.10	0	1	0.6162	1	704	1.00	324	19.00
0.7–1.0	3.80	350	201	−0.001	4.00	417	0.10	0	1	0.1932	1	190	4.06	470	19.85
1.0–1.5	4.05	400	199	−0.0016	4.00	291	0.10	0	1	0.0522	1	265	3.25	704	20.29
1.5–2.0	4.15	380	175	−0.0026	4.00	291	0.10	0	1	0.0092	1	144	2.83	1293	20.50
2.0–3.0	4.20	342	151	−0.0031	4.00	276	0.10	−19	10	0.0088	1	417	17.34	1393	20.60
3.0–4.0	4.20	298	129	−0.0042	4.00	338	0.10	−41	22	0.1238	1	1000	1.23	1247	20.60
4.0–6.0	4.15	246	107	−0.0047	4.00	342	0.10	−51	30	0.3361	1	1000	1.69	2396	20.24
6.0–8.0	4.00	174	79	−0.0058	4.00	337	0.10	−50	41	0.0000	1	466	2.46	3221	21.45

Last column (the site term) varies by station (site term can be found in Ⓔ Table S1, available in the electronic supplement to this article).

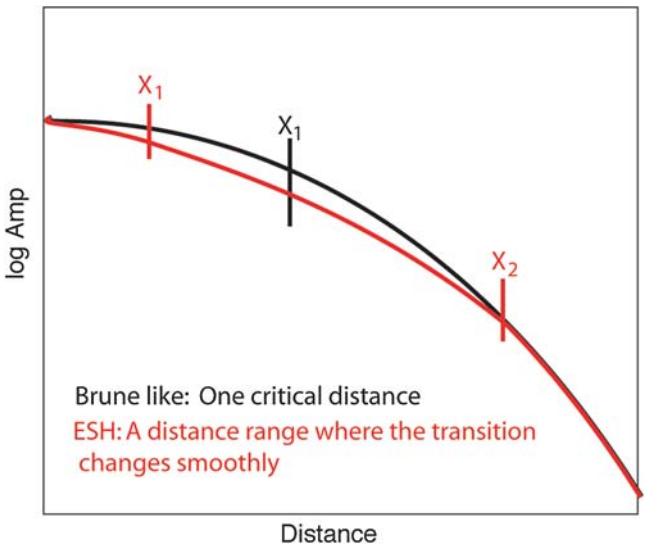

Figure 5. A comparison of the Extended Street and Herrmann (ESH) formulation (red) with two critical distances to a single critical distance (black).

$$X_1 = X_c/X_t \qquad X_2 = X_c \times X_t, \tag{7}$$

in which X_c is the critical distance and X_t is the transition term. These terms and p_1, p_2 are provided in Table 1. As shown in coda shape parameter plots, variability of the coda shape function is higher at local distances ($\Delta < 200$ km), specifically at higher frequencies which indicates a difference between local *S*-wave coda and regional *Lg* coda.

We determined the path correction by inverting the measured coda amplitudes for three parameters (p_1, X_1, and X_2), in which p_2 is fixed (Fig. 5). Figure 6 shows one frequency band and the path distribution in which we obtained those correction parameters. The number of paths is more limited than the number of paths shown in Figure 2 (peak velocity measurement), due to earthquake distribution, rejected measurements, or not having enough measurements for a common earthquake recorded by two or more stations. The majority of paths are within the 500–800-km distance range.

We apply these empirical corrections to the coda amplitudes in each frequency and obtain dimensionless amplitudes. The next step is to tie this to known M_w measurements calculated in the region through independent techniques, such as 1D long-period waveform modeling. Figure 7 illustrates how *S*-to-coda transfer is applied to obtain site terms (Table 1, Site; Ⓔ Table S1) using station UOSS and source spectra. We use moment estimates from Gene Ichinose (personal comm., 2016) and Covellone and Savage (2012). Ichinose uses a specific velocity model to the region for waveform inversion, whereas Covellone and Savage (2012) use an adjoint tomography method in which they improved the model during moment tensor inversion. We compared common events obtained using both techniques to examine any bias. The M_w values were quite consistent without any bias and little scatter. It is known that an unrepresentative regional velocity model can cause under or overestimation of the moment value (e.g., Patton and Randall, 2002). We believe that these 168 independently waveform-modeled events are reliable estimates of the moment magnitudes in the Middle East region.

Theoretical source spectra created using the MDAC (magnitude, distance, amplitude correction) (Walter and Taylor, 2001) formulation are applied, and the site correction is obtained at each frequency band using reference seismic moments obtained from waveform modeling (Fig. 7). The MDAC methodology creates a synthetic moment-rate spectra using a simple earthquake source model to observed regional seismic spectra. We used MDAC parameters for which the apparent stress and reference moment are 0.3 MPa and 0.30×10^{16} N·m, respectively. Obviously, a bias can be introduced during calibration. For now we ignore these effects, because the result will be observed in higher-frequency portion of the source spectra. The moment magnitudes for the rest of the events are obtained using an MDAC fit in which the spectrally derived moment is converted to moment magnitude using the relation: $M_w = (2/3) \times (\log(M_0) - 16.1)$ (Hanks and Kanamori, 1979).

Results

We obtained moment magnitude estimates of 2247 crustal events in the Middle East region using the 1D coda calibration, in which the calibration parameters are listed in Table 1. The range of magnitudes spans from small to very large events ($3.5 < M_w < 7.0$) (Ⓔ Table S2). As shown in the velocity peak values in Figure 2, our fitted hyperbola (red line) is averaging the distributed *Sn* and *Lg* phase velocities specifically at frequencies between 0.7 and 1.5 Hz. This may clearly introduce an error in our measurements. To illustrate the possible effect of this issue, we show the 11 November 2006 M_w 4.09 event as an example of fit to the various frequencies using the coda calibration technique (Fig. 8). Stations KRBR and GRMI are at similar epicentral distances, but the GRMI path travels along the northern Zagros (where *Sn* is observed), whereas KRBR path travels through the central Iranian plateau. Similar to Figure 4a, we see variations in the envelopes. This variation, however, does not show a very significant effect on the source spectra (Fig. 9b) below 0.7 Hz. In some cases such as Figure 9a, more variations are at higher frequencies, which might be due to 2D attenuation effects. Instead of limiting our MDAC fit to the observed moment-rate spectra below a certain frequency, we fit the full spectra and document the frequency range that the low-frequency spectral level (thus M_w) is calculated from.

Nonetheless, the flat low-frequency part of the moment-rate spectra for which the M_w is measured is around 1 Hz for $M_w \geq \sim 3.5$. The comparison of 168 calibration events with coda-derived M_w values is shown in Figure 10a. Higher scattering is still observed at $4.0 < M_w < 5.0$ than at large magnitudes, and this is expected, due to the 2D variations of regional coda shapes and amplitudes having a stronger effect above 0.7 Hz. The correlation is high, does not show much

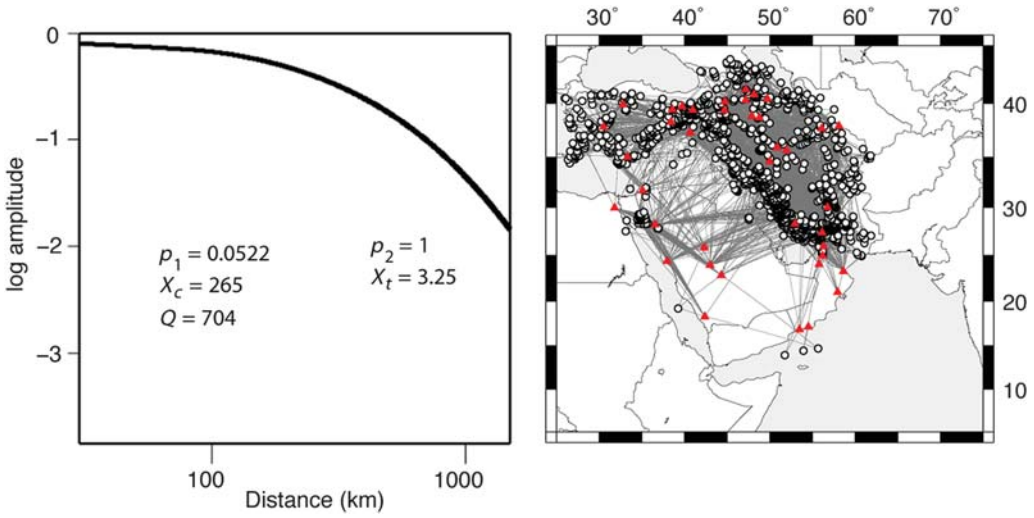

Figure 6. 1D path (ESH) correction curve (left) for frequencies 0.7–1.0 Hz with the path coverage on the right.

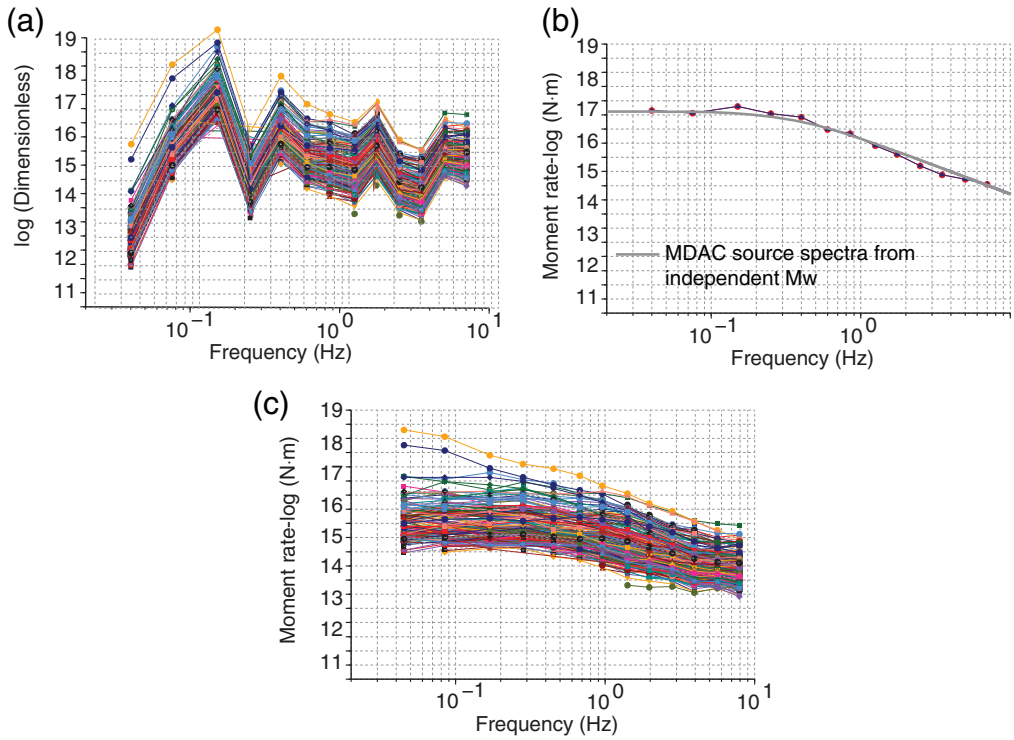

Figure 7. (a) Source spectra site corrections are illustrated using 360 path-corrected amplitudes at station UOSS, (b) one independent waveform-modeled event is shown as an example out of 168 calibration events that contributed to the site corrections (Table 1), and (c) moment-rate spectra of the site-corrected amplitudes. Note the higher corner-frequency level of small events.

scatter, and shows no bias. The standard deviation of single-station spectra is calculated for these calibration events, and the results are shown in Figure 10b. The average standard deviation is 0.25 for frequencies between 0.03 and 0.5 Hz, whereas it increases as high as 0.4 at frequencies >0.7 Hz.

Results of four selected events representing selected regions are shown in Figure 9. In Figure 9a, event source spectra are shown from the southern Zagros (SZ). The dashed gray line is the MDAC spectra for an M_w 4.21 event. Four different stations are located in the Zagros, Makran, and the Persian Gulf, ranging from a few hundred kilometers to larger epicentral distances. Source spectra from individual stations show scatter above 1.0 Hz. Figure 9b is from an event in central Zagros (CZ), where the recording stations span most of the Iranian plateau. This M_w 4.09 event does not have many high-frequency measurements, due to strong attenuation. The source spectra shown in Figure 9c are from an event in the Caucasus. This event was recorded by the Iranian, Turkish, and Global

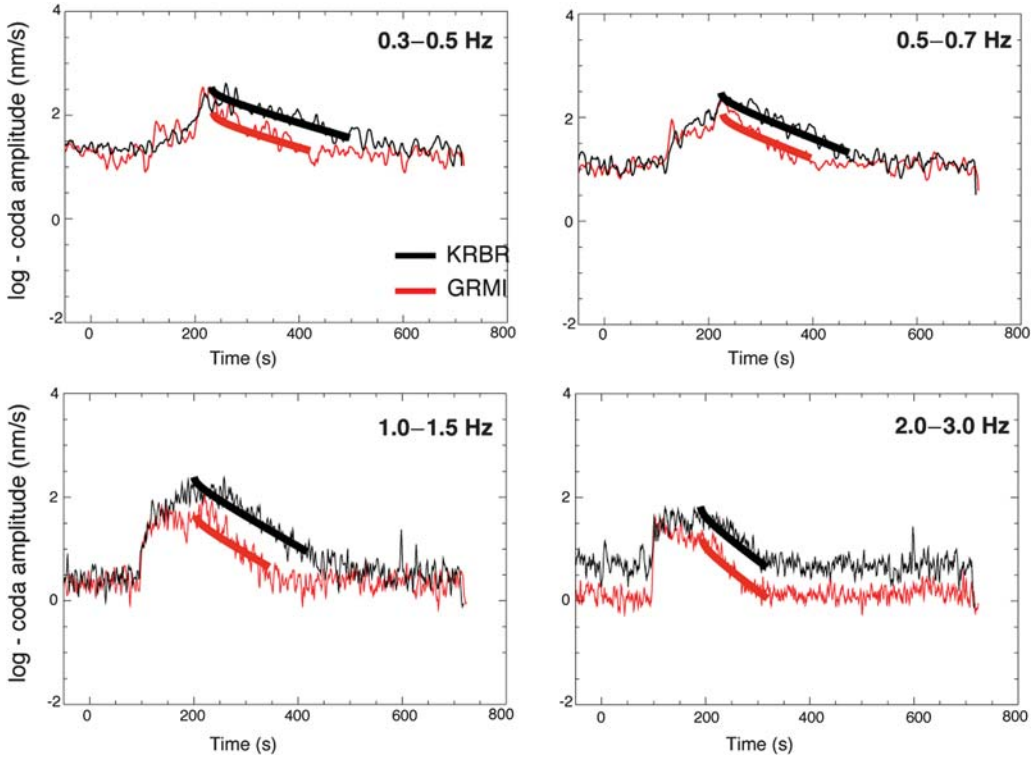

Figure 8. Synthetic and raw coda envelopes are displayed for four frequency bands. In order to illustrate the coda shape effect, we picked two stations that are fairly close in their epicentral distances: KRBR is 721 km and GRMI is 732 km (stations are located in opposite azimuths). Here, we see that for the higher frequencies the fitting of the envelopes is degraded, as is the predicted onset of the coda because the peak velocity is somewhat of an average between *Sn* and *Lg* peak velocities (Fig. 9b, central Zagros [CZ]).

Seismographic Network (GSN-IRIS) stations. High-frequency scatter of the source spectra is larger for this event above the 0.5–0.7 Hz band. The paths to this event propagate through the Greater Caucasus (KIV), Lesser Caucasus (AGRB), Anatolian plateau (VANB, URFA), and the Iranian plateau (NASN, SHGIR, GHIR). The independent waveform modeling M_w solution of this event is overestimated at 5.01. Our coda calibration results in a very consistent estimate of M_w 4.70. If the regional models are inappropriate or the 3D variations are strong, the regional moment tensor solutions can be significantly affected. The last example shows an event from eastern Turkey. The IRIS-PASSCAL deployment in eastern Turkey recorded this event as well as the GSN-IRIS stations (KIV, ISP, and CSS). For this event, the source spectra show larger variation above 0.5 Hz. The path to CSS travels partially through the Mediterranean. This may cause a conversion at the continental/oceanic crust boundary (Gök *et al.*, 2000).

The standard deviations that are shown in Figure 10b are the basis for error bounds for the magnitudes that are provided in this study. In the table of magnitudes, we provide the frequency range of the flat portion of the source spectra in which M_w is measured and the number of stations for each event, so that the user can carefully evaluate the quality of the magnitude estimate. Because of the limited number of stations in the early years, we kept the criteria for the minimum number of stations to average for M_w to at least one, and the minimum number of frequency measurements for each spectrum to be four. The magnitude for each event is obtained by fitting the MDAC source spectra to the station-averaged source spectra at each individual frequency.

Magnitude Relationship

Local magnitudes of national networks and PSHA studies often require stable M_w measurements in order to obtain the completeness and harmonization of the catalogs (T. Onur *et al.*, unpublished manuscript, 2016; see Data and Resources section). We derived the relationship between coda M_w and M_L, m_b, and M_s magnitudes. Because each event reported in the catalogs often had magnitude estimates from several different organizations, we use the median value from the available catalogs. Instead of a least-squares fit to the data, which requires that the uncertainty on the independent variable (i.e., M_L, m_b, and M_s) is at least one order of magnitude smaller than the one on the dependent variable (i.e., M_w), we utilize orthogonal regression. This method allows both the dependent and independent variables to be affected by uncertainty (Kendall and Stuart, 1979; Castellaro *et al.*, 2006). Figure 11 shows the relationship between these magnitudes. The red line is the orthogonal fit and is shown along with the dashed line, which is a linear fit.

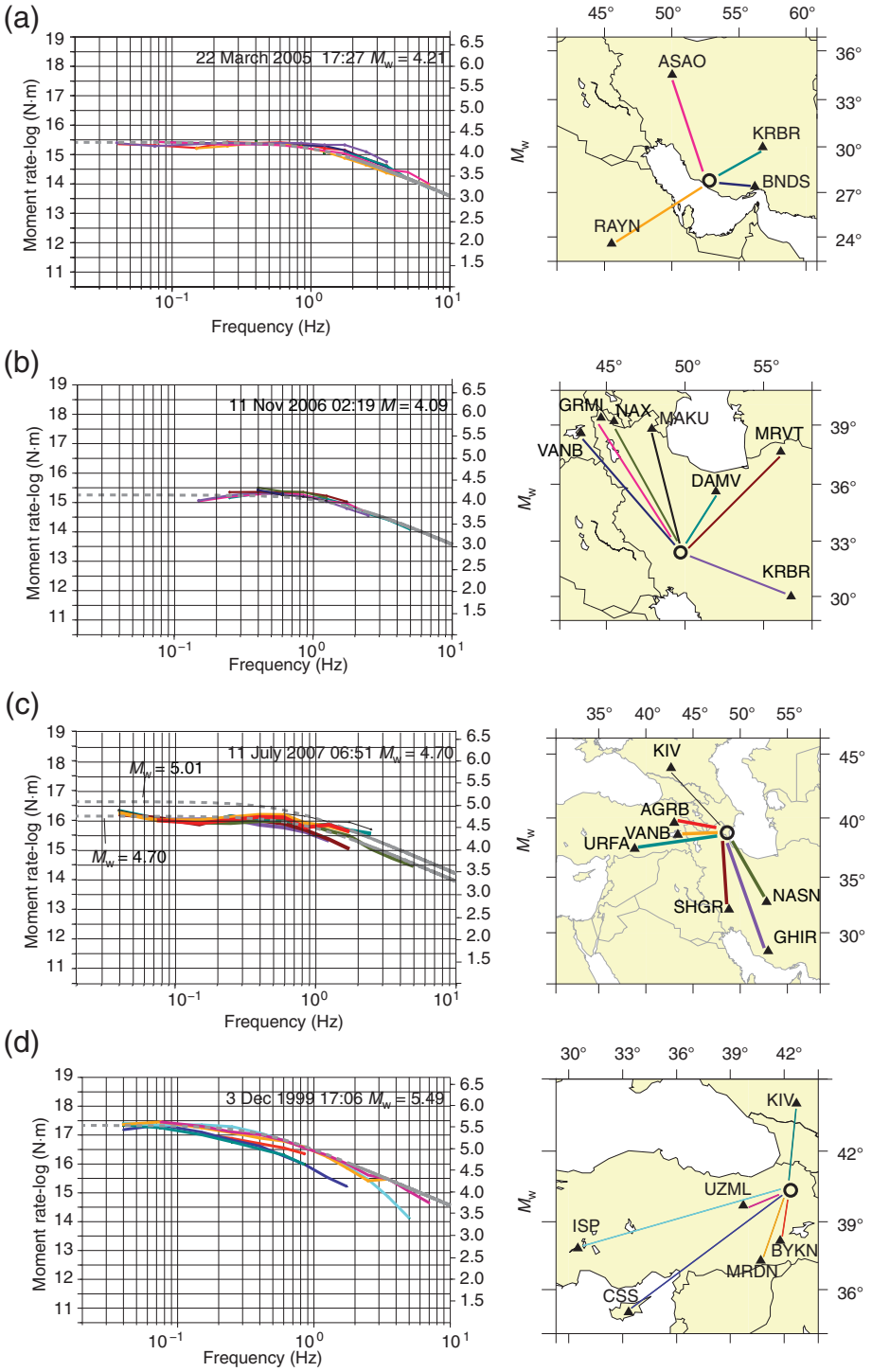

Figure 9. Selected four events with source spectra at individual stations shown with source spectra from calibrated events at (a) SZ (event from Fig. 4a), (b) CZ, (c) Caucasus–Caspian (CC) (M_w 5.01 is from waveform-modeled M_w), and (d) eastern Turkey (ET). Magnitudes shown at panels are derived from coda envelopes. The gray dashed line is magnitude, distance, amplitude correction (MDAC) theoretical source spectra.

Conclusion

Although we observe significant variations in the seismograms throughout the region, the 1D coda method has shown the ability to provide stable moment estimates for frequencies below ~0.7 Hz and subsequently is ideal for the moderate-to-large magnitude events (~3.5 < M_w < 7.0). The technique allows us to measure M_w values down to 2.0, with increasing variations at higher frequencies (Fig. 10b) increasing the uncertainty in the measure. In addition, the shorter coda lengths for smaller events may be dominated by more forward multiple scattering than the back scattering expected in longer

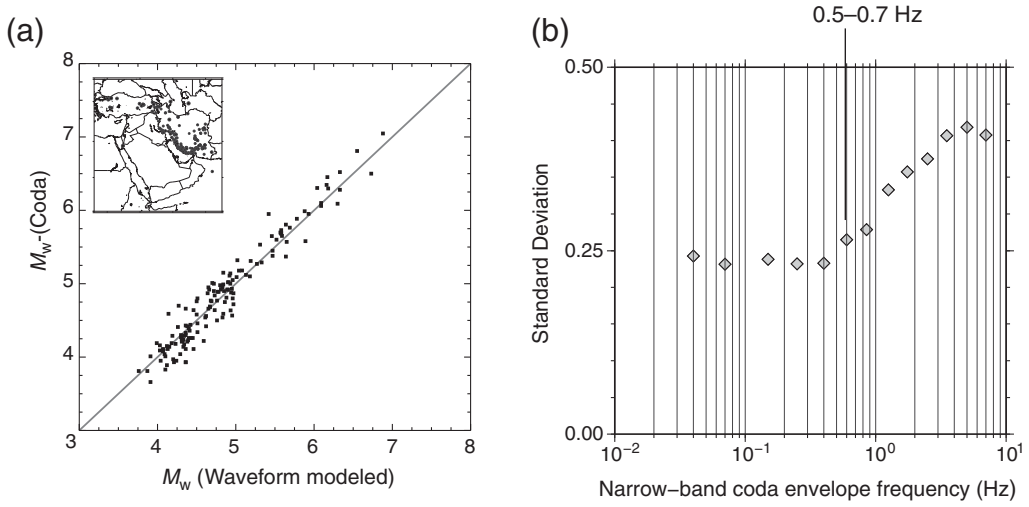

Figure 10. (a) Coda M_w comparison of 168 events with waveform-modeled M_w (no bias is observed). (b) Standard deviations grouped in different frequency bands. The average standard deviation is 0.25 for frequencies between 0.03 and 0.5, whereas it increases as high as 0.4 at frequencies >0.7 Hz.

duration coda. For the events reported in the Ⓔ electronic supplement, we prefer to provide the estimates with the lowest uncertainty, and so have limited those to magnitudes of 3.5 and greater. Given the limitations for smaller events, we provide information on the range of frequencies (Ⓔ Table S2 low frequency, high frequency) and the number of stations used in the Ⓔ electronic supplement to allow users to assess the quality of the results. Because many network operators are interested in analyzing events smaller than M_w 3.5, we provide guidelines in the Ⓔ electronic supplement to judiciously apply window lengths for smaller events at higher frequencies using fewer stations. Currently, only a very limited amount of moment magnitudes are available in the Middle East, and this study provides for the first time moment magnitudes of many smaller events in the region. We also investigated the energy–moment relationship for the reported events by calculating energy from the coda-derived source spectra. We initially observed a nonconstant scaling between energy and moment.

In a companion paper (Pasyanos *et al.*, 2016), we will demonstrate the ability to better resolve higher-frequency coda measurements using 2D path corrections. That paper uses the 1D results derived here as an initial model and a different technique to address the 2D coda-derived source spectral path corrections. The resulting variable attenuation structure can be used to robustly estimate the magnitudes of small events, using only high frequencies and at only a few paths or a single path. This reduces the variance of the magnitude estimates for small events and will enable the determination of robust moment magnitudes <3.5.

Traditional magnitudes (e.g., M_L, m_b, and M_s) are most sensitive to certain frequency ranges. For large events at longer distances, almost all magnitudes saturate above 20 s. M_s can be used for larger events at longer distances, but it is sensitive to depth and radiation pattern. M_L and m_b are obtained from higher frequencies ($\sim$1.0 Hz) of certain phases on the seismogram. These types of magnitudes are traditionally reported in bulletins and catalogs for local-to-regional distances. They will clearly be sensitive to attenuation and 2D variation along the path or phase variation (e.g., *Lg*, *Sn*). Consequently, these specific magnitudes will not be an accurate measure for the actual size of the event. For the completeness and harmonization, magnitude relationships provide important constraints in seismic-hazard studies, such as how accurate M_w values can contribute to the Gutenberg–Richter relationship. The Gutenberg–Richter magnitude–frequency slope (b) will vary depending on how well the smaller event magnitudes are measured. This study provides a basis for accurate estimates of M_w over a wide range of event sizes and recording distances throughout the Middle East and thus provides a strong basis for regional PSHA studies and other studies that require a magnitude relationship for the moment magnitudes.

One of our goals in this article is to support the operational needs of national networks in the Middle East region. With developing networks and seismic data availability, regional models are improving but are still not quite adequate to predict Green's functions to be used for routine regional moment tensor inversion and moment magnitude studies. At Lawrence Livermore National Laboratory (LLNL), we developed a Java-based application named The Seismic Wave-Form Tool (SWFT) to speed the measurement of M_w values through the coda calibration technique described here. The code is available upon request and uses Seismic Analysis Code (SAC) format data. The calibration presented here will help local monitoring organizations perform rapid moment magnitude determinations.

Data and Resources

Data are obtained from the Incorporated Research Institutions for Seismology-Program for the Array Seismic Studies of the Continental Lithosphere (IRIS-PASSCAL)

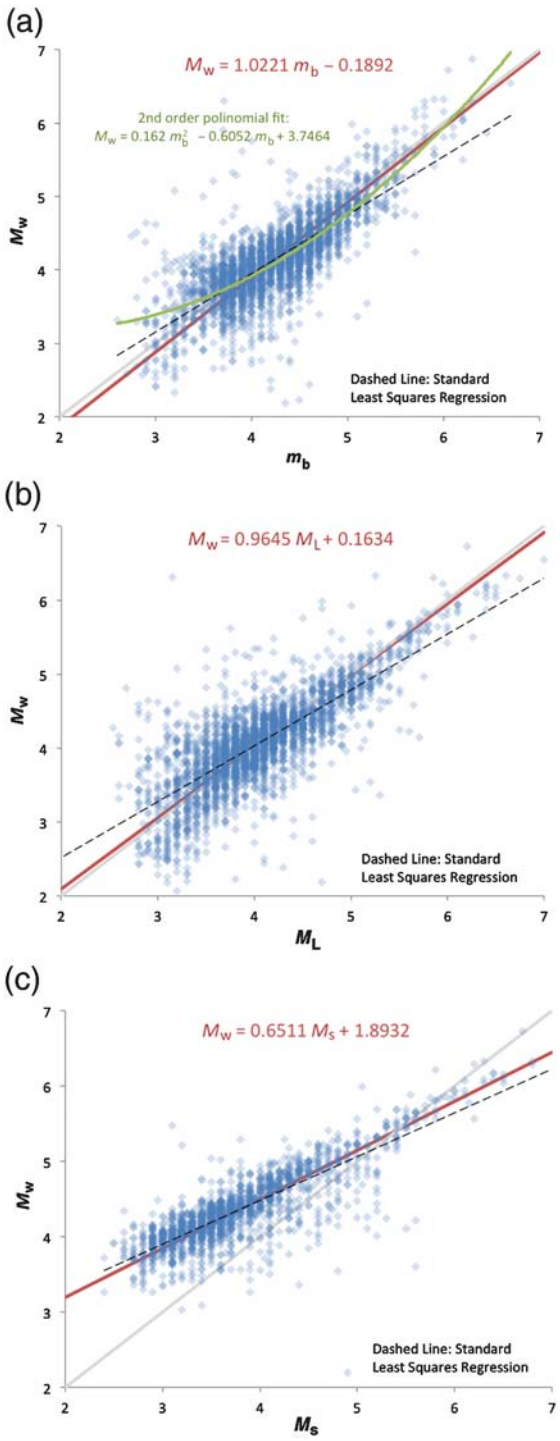

Figure 11. Relationship between coda M_L, m_b, and M_s. The red line and the equation in red is the orthogonal fit, the black-dashed line is a linear fit. The green line shows the second-order polynomial fit only for $m_b - M_w$.

deployments, International Institute of Earthquake Engineering and Seismology (IIEES), Republic Seismic Survey Center of Azerbaijan (RCSS), Earthquake Monitoring Center (EMC) of Sultan Qaboos University, King Abdullah City of Science and Technology (KACST), Kandilli Observatory and Earthquake Research Institute (KOERI), Kuwait Institute of Scientific Research (KISR), and Saudi Geological Survey (SGS). The unpublished manuscript "Unified seismic catalog of Iraq," by T. Onur, R. Gök, H. Mahdi, and H. Al-Shukri (2016), has been submitted to *Seismological Research Letters*.

Acknowledgments

The majority of the openly available data are obtained from Incorporated Research Institutions in Seismology (IRIS). Plotting is done using Generic Mapping Tool (GMT) macros. This work was performed under the auspices of the U.S. Department of Energy by Lawrence Livermore National Laboratory under Contract Number DE-AC52-07NA27344. This study is partially supported by Air Force Research Laboratory (AFRL) FA9453-11-C-0235 and DE-AC52-07NA27344/LL11-BAA11-13-NDD03. This is Lawrence Livermore National Laboratory (LLNL) Contribution Number LLNL-JRNL-679299.

References

Aki, K., and B. Chouet (1975). Origin of coda waves: Source, attenuation, and scattering effects, *J. Geophys. Res.* **80,** 3322–3342.

Al-Damegh, K., E. Sandvol, A. I. Al-Lazki, and M. Barazangi (2004). Regional seismic wave propagation (*Lg* and *Sn*) and *Pn* attenuation in the Arabian plate and surrounding regions, *Geophys. J. Int.* **157,** 775–795.

Baumgardt, D. R. (2001). Sedimentary basins and the blockage of *Lg* wave propagation in the continents, *Pure Appl. Geophys.* **158,** 1207–1250.

Castellaro, S., F. Mulargia, and Y. Y. Kagan (2006). Regression problems for magnitudes, *Geophys. J. Int.* **165,** 913–930.

Cong, L., and B. Mitchell (1998). *Lg* coda *Q* and its relation to the geology and tectonics of the Middle East, *Pure Appl. Geophys.* **153,** 2/4, 563–585.

Covellone, B., and B. Savage (2012). A quantitative comparison between 1D and 3D source inversion methodologies: Application to the Middle East, *Bull. Seismol. Soc. Am.* **102,** no. 5, 2189–2199.

Eken, T., K. Mayeda, A. Hofstetter, R. Gök, G. Orgülu, and N. Turkelli (2004). An application of the coda methodology for moment-rate spectra using broadband stations in Turkey, *Geophys. Res. Lett.* **31,** L11609, doi: 10.1029/2004GL019627.

Favreau, P., and R. J. Archuleta (2003). Direct seismic energy modelling and application to the 1979 Imperial Valley earthquake, *Geophys. Res. Lett.* **30,** 1198.

Gök, R., E. Sandvol, N. Türkelli, D. Seber, and M. Barazangi (2003). *Sn* attenuation in the Anatolian and Iranian plateau and surrounding regions, *Geophys. Res. Lett.* **30,** no. 4, 8042, doi: 10.1029/2003GL018020.

Gök, R., N. Turkelli, E. Sandvol, D. Seber, and M. Barazangi (2000). Regional wave propagation in Turkey and surrounding regions, *Geophys. Res. Lett.* **27,** no. 3, 429–432.

Hanks, T. C., and H. Kanamori (1979). A moment magnitude scale, *J. Geophys. Res.* **84,** 2348–2350.

Jin, A., and K. Aki (1988). Spatial and temporal correction between coda *Q* and seismicity in China, *Bull. Seismol. Soc. Am.* **78,** 741–769.

Jin, A., and K. Aki (2005). High-resolution maps of coda *Q* in Japan and their interpretation by the brittle-ductile interaction hypothesis, *Earth Planets Space* **57,** 403–409.

Kadinsky-Cade, K., M. Barazangi, J. Oliver, and B. Isacks (1981). Lateral variations of high-frequency seismic wave propagation at regional distances across the Turkish and Iranian plateaus, *J. Geophys. Res.* **86,** doi: 10.1029/JB086iB10p09377, ISSN 0148–0227.

Kaviani, A., E. Sandvol, X. Bao, G. Rümpker, and R. Gök (2015). The structure of the crust in the Turkish-Iranian plateau and Zagros using *Lg Q* and velocity, *Geophys. J. Int.* **200,** no. 2, 1254–1268, doi: 10.1093/gji/ggu468.

Kendall, M. G., and A. Stuart (1979). *The Advanced Theory of Statistics*, Vol. 2, Fourth Ed., Griffin, London, United Kingdom.

Malagnini, L., K. Mayeda, A. Akinci, and P. L. Bragato (2004). Estimating absolute site effects, *Bull. Seismol. Soc. Am.* **94,** no. 4, 1343–1352.

Mayeda, K. (1993). m_b (*Lg* coda): A stable single station estimator of magnitude, *Bull. Seismol. Soc. Am.* **83,** 851–861.

Mayeda, K., and L. Malagnini (2010). Source radiation invariant property of local and near-regional shear-wave coda: Application to source scaling for the M_w 5.9 Wells, Nevada sequence, *Geophys. Res. Lett.* **37,** L07306, doi: 10.1029/2009GL042148.

Mayeda, K., and W. R. Walter (1996). Moment, energy, stress drop, and source spectra of western United States earthquakes from regional coda envelopes, *J. Geophys. Res.* **101,** 11,195–11,208.

Mayeda, K., A. Hofstetter, J. L. O'Boyle, and W. R. Walter (2003). Stable and transportable regional magnitudes based on coda-derived moment-rate spectra, *Bull. Seismol. Soc. Am.* **93,** 224–239.

Mitchell, B. J., Y. Pan, J. Xie, and L. Cong (1997). *Lg* coda *Q* variation across Eurasia and its relation to crustal evolution, *J. Geophys. Res.* **102,** no. B10, 22,767–22,779.

Molnar, P., and J. Oliver (1969). Lateral variations of attenuation in the upper mantle and discontinuities in the lithosphere, *J. Geophys. Res.* **74,** 2648–2682.

Morasca, P., K. Mayeda, R. Gök, W. S. Phillips, and L. Malagnini (2008). 2D coda and direct-wave attenuation tomography in northern Italy, *Bull. Seismol. Soc. Am.* **98,** no. 4, 1936–1946.

Pasyanos, M. E., R. Gök, and W. R. Walter (2016). 2-D variations in coda amplitudes in the Middle East, *Bull. Seismol. Soc. Am.* **106,** no. 5, doi: 10.1785/0120150336.

Patton, H. J., and G. E. Randall (2002). On the causes of biased estimates of seismic moment for earthquakes in central Asia, *J. Geophys. Res.* **107,** doi: 10.1029/2001JB000351.

Rodgers, A. J., J. F. Ni, and T. M. Hearn (1997). Propagation characteristics of short-period *Sn* and *Lg* in the Middle East, *Bull. Seismol. Soc. Am.* **87,** 396–413.

Sandvol, E., K. Al-Damegh, A. Calvert, D. Seber, M. Barazangi, R. Mohamad, R. Gök, N. Turkelli, and C. Gurbuz (2001). Tomographic imaging of *Lg* and *Sn* propagation in the Middle East, *Pure Appl. Geophys.* **158,** 1121–1163, doi: 10.1007/PL00001218.

Singh, S., and R. B. Herrmann (1983). Regionalization of crustal coda *Q* in the continental United States, *J. Geophys. Res.* **88,** 527–538.

Street, R. L., R. B. Herrmann, and O. W. Nuttli (1975). Spectral characteristics of the *Lg* wave generated by central United States earthquakes, *Geophys. J. Roy. Astron. Soc.* **41,** 51–63.

Walter, W. R., and S. R. Taylor (2001). A revised Magnitude and Distance Amplitude Correction (MDAC2) procedure for regional seismic discriminants: Theory and testing at NTS, Lawrence Livermore National Laboratory, UCRL-ID-146882, 13 pp.

Yoo, S.-H., J. Rhie, H.-S. Choi, and K. Mayeda (2011). Coda-derived source parameters of earthquakes and their scaling relationships in the Korean Peninsula, *Bull. Seismol. Soc. Am.* **101,** 2388–2398, doi: 10.1785/0120100318.

Lawrence Livermore National Laboratory
7000 East Avenue L-049
Livermore, California 94550
gok1@llnl.gov
(R.G., E.M.M., M.E.P., W.R.W.)

Institute of Geosciences
Goethe University of Frankfurt
Altenhoeferallee 1
D-60438 Frankfurt, Germany
(A.K.)

EECS
University of California, Berkeley
253 Cory Hall
Berkeley, California 94720
(K.M.)

Azerbaijan National Academy of Sciences
Republican Seismic Survey Center of Azerbaijan
National Academy of Sciences
25, Nigar Rafibeyli Street
AZ1001, Baku, Azerbaijan
(G.Y.)

Earthquake Monitoring Center
Sultan Qaboos University
PO Box 50, PC 123
Al Khoud, Sultanate of Oman
(I.E.-H.)

King Saud University
Riyadh 11451, Kingdom of Saudi Arabia
(A.A.-A.)

Kuwait Institute of Scientific Research
P.O. Box 24885
Safat 13109
Kuwait City, Kuwait
(F.A.-J.)

Ilia State University
Shalva Nutsubidze Street
Tbilisi, Georgia
(T.G.)

Kandilli Observatory and Earthquake Research Institute
34684 Çengelköy
İstanbul, Turkey
(D.K.)

University of Missouri
Department of Geological Sciences
101 Geology Building
Columbia, Missouri 65211-1380
(E.A.S.)

Manuscript received 12 February 2016;
Published Online 13 September 2016